March 2006

Raghavan, V., Gogos, G., Babu, V. and Sundararajan, T., "Effect of Gravity on Methanol Diffusion Flames Burning within a Forced Convective Environment", accepted for publication in International Communications in Heat and Mass Transfer (2006)

Effect of Gravity on Methanol Diffusion Flames Burning Within a Forced Convective Environment

V. Raghavan, George Gogos*
Department of Mechanical Engineering,
University of Nebraska-Lincoln, Lincoln, NE, 68588, USA
V. Babu and T. Sundararajan
Department of Mechanical Engineering,
Indian Institute of Technology Madras, Chennai, Tamilnadu, 600036, INDIA

Abstract

Characteristics of methanol diffusion flames burning under three different configurations with respect to the directions of forced and natural convective flow fields are presented for zero and normal gravity conditions. Combustion of a spherical methanol particle and of a methanol film within a mixed convective environment, have been numerically simulated. The effects of gravity on aiding, opposing and perpendicular flow are presented. The gravitational field considerably changes the flow field, flame shapes and fuel burning rates, especially for the opposing flow case.

Keywords: methanol, combustion, diffusion flames, buoyancy, forced convection

1 Introduction

Gravity affects flames through buoyancy-induced flow. The gravitational field creates a strong buoyancy flow in the opposite direction of the gravitational vector, due to relative temperature differences. The interaction between a forced convective flow and buoyancy-induced flow produces interesting burning characteristics. Three different configurations with respect to the directions of buoyancy and forced convective flow fields have been considered, which are shown in Fig. 1. In the first two configurations, the forced convective flow is parallel to the buoyancy flow. However, they can be either in the same direction (aiding flow) or in the opposite direction (opposing flow). In the third configuration, the forced convective flow is perpendicular to the buoyancy flow (perpendicular flow). For the first two configurations, quasi-steady burning of an isolated spherical methanol particle in a mixed convective environment has been considered and for the third configuration, quasi-steady combustion of a methanol film off a flat plate (classical Emmons problem [1]) has been considered. Quasi-steady combustion models for the burning of stationary spherical particles have been developed in the past for isolated liquid fuel droplets [2 – 5], in which the transport processes inside the particles are neglected. These quasi-steady models are applicable for the low pressure burning of fuel particles, after the initial ignition and internal heating transients are over. Verification for the quasi-steady burning of an isolated, spherical fuel particle has been carried using the porous sphere technique [6, 7]. Recently, Balakrishnan et al. [8], Pope and Gogos [9] and Raghavan et al. [10] investigated the quasi-steady burning of an isolated spherical particle in a convective environment. Transient analysis of the effect of natural convection on high pressure droplet combustion has been carried out by Sato et al. [11]. Single droplet combustion within a gravitational environment over a wide range of gravity strength (0g to 10g) has been presented by Ling and Chiun [12]. Balakrishnan et al. [8] and Raghavan et al. [10] have presented flame shapes for both aiding flow

* Corresponding Author: Email: ggogos1@unlnotes.unl.edu, Phone: (402)-472-3006, Fax: (402)-472-1465

and opposing flow cases. However, for the opposing flow case, only the envelope flame regime has been presented [10].

Combustion of a liquid fuel film off a flat plate has been investigated by Emmons [1]. Velocity distribution in the boundary layer over a flat plate with diffusion flame has been measured by Hirano et al. [13]. Temperature measurements on a boundary layer diffusion flame have been reported by Brahmi et al. [14]. Investigations on the stability and extinction of a laminar diffusion flame over a porous plate have been carried out by Ramachandra and Raghunandan [15]. These investigators give details about the flame quenching due to forced convection strength and fuel supply rate. Li et al. [16] have investigated experimentally the variation of the flame anchoring position with freestream velocity.

2 Numerical Model

The salient features of the numerical model are: (a) non-orthogonal control volumes with semi-collocated mesh, (b) generalized interpolation of all the flow and transport variables in a cell, (c) finite rate chemistry and (d) detailed evaluation of thermo-physical properties based on local temperature and species concentrations. Numerical results have been obtained for a range of mixed convective flow conditions.

The simulations have been carried out with the following simplifications:

1. The flow is laminar. It is assumed axi-symmetric for the aiding and the opposing flow problems and 2D for the perpendicular flow problem.
2. Ideal-gas mixture formulation is used to account for density variations with temperature and concentration. However, the incompressible flow solution methodology has been adopted to derive the pressure field, as the flow velocities are considerably less than the speed of sound.
3. Only the gas phase region has been modeled in a decoupled manner, assuming no slip boundary condition at the particle or film surface and no liquid-phase heating effects are considered. These approximations are applicable to the low pressure burning of a fuel particle or a fuel film, during the quasi-steady burning period.
4. Single component fuel undergoing complete combustion through a global reaction step has been considered. Only gas-phase combustion is studied, which amounts to assuming high fuel volatility.
5. Chapman–Enskog description for binary gas mixtures has been used to evaluate thermo-physical properties such as thermal conductivity and viscosity. Piecewise polynomials in temperature have been used to evaluate specific heats and species enthalpies.
6. Thermal radiation effects are neglected, which amounts to assuming a non-luminous flame.
7. The partial pressure of vapor adjacent to the particle or film surface is assumed to be equal to the vapor pressure of the fuel at the interface temperature. Thus, the fuel mole fraction adjacent to the particle or film surface can be written using the Clausius-Clayperon equation.

Local evaporation velocity at particle or film surfaces have been evaluated using the fact that the total fuel mass flow rate at the surface is equal to the sum of the fuel mass flow rates due to convection and diffusion. A theoretical analysis incorporating the above assumptions can be employed primarily for modeling the quasi-

steady burning of liquid fuel particles or films, and for the combustion of solid fuel particles to a limited extent (when combustion occurs in the gas phase alone). Details of the governing equations, boundary conditions, evaluation of thermo-physical properties and reaction rates and detailed solution procedure are given in Raghavan et al. [10].

The numerical model with methanol as the liquid fuel has been thoroughly validated [10] and has been used in the simulations of the first two cases (aiding and opposing flow problems). For the third case (perpendicular flow problem), the model has been modified to solve the governing equations and boundary conditions in 2D Cartesian coordinates (z, y) (see Fig. 1c), instead of axi-symmetric cylindrical polar coordinates (r-x). Here, the gravity acts in the negative y direction. The ambient temperature and pressure have been 300 K and 1 bar for all the simulations. Cases with zero gravity and normal gravity have been simulated.

3 Results and Discussion

Case 1: Aiding Flow

In this case, a spherical methanol particle of 8 mm in diameter, undergoing combustion within a mixed convective environment with the buoyancy flow being aided by the forced convective stream of air has been considered (see Fig. 1a). The freestream velocities have been varied from 0.3 to 2 m/s. The corresponding freestream Reynolds numbers based on particle diameter are in the range of 150 to 1000. Figure 2a shows the flame shapes for zero gravity and normal gravity cases at a freestream velocity of 0.4 m/s. At this freestream velocity, the flame envelopes the particle. The contour lines corresponding to the oxygen mass fractions of 0.002 to 0.02 have been used to represent the combustion zone in this study [10]. Figure 2b shows the variation of the flame stand-off distances in the envelope flame regime (u_∞ from 0.3 to ~0.8 m/s) with the freestream velocity. Both h_1 and h_2 are flame distances from the particle surface (see Fig. 1a). The flame stand-off distances decrease for both cases as the freestream velocity increases. The case with zero gravity has larger flame stand-off distances because the flame in the normal gravity environment is stretched further by the buoyancy-induced flow field. As the freestream velocity is increased, the differences in the flame stand-off distances between the cases with and without gravity decrease. Before transition to wake flames, the flame stand-off distances at the front stagnation point (h_1) for both cases are the same and approximately 0.9 mm. This value is consistent with the literature [9, 17 & 18].

As the freestream velocity is increased to approximately 1 m/s, transition from envelope flame to wake flame occurs for the normal gravity case. Extinction of the flame in the front portion of the sphere occurs, because the flow residence time is less than the reaction time. The flame is established in the wake region where the residence time for the reactants is longer due to recirculation caused by flow separation. Due to the absence of the buoyant flow field, which results in smaller flame stretching, the case with zero gravity retains an envelope flame. Figure 3a illustrates this fact. At a higher freestream velocity ($u_\infty \approx 1.1$ m/s), transition from envelope flame to wake flame occurs for the case with zero gravity as well (see Fig. 3b). However, the flame is stabilized in the boundary layer in the rear portion of the particle for the case with normal gravity, while the flame is stabilized in the wake region for the case with zero gravity. At a still higher freestream velocity ($u_\infty \approx 2$

m/s), for both the cases, the flame stabilizes in the wake region (see Fig. 3c). The variation of the flame height with the freestream velocity is shown in Fig. 3d. The flame height (h_3/d) (see Fig.1a) is measured from the particle surface. Obviously, due to additional flame stretching, the case with normal gravity has larger flame height than the case with zero gravity, except during transition.

The flow field changes considerably due to the effect of gravity. Figures 4(a-d) illustrate the streamlines for the cases with zero and normal gravity, at different freestream velocities. The boundary layer for the case with normal gravity is thinner than that with zero gravity. Also, at freestream velocities higher than the ones corresponding to the transition regime, the recirculation wake region is larger for the case with zero gravity.

The variation of the mass burning rate (kg/s) with the freestream velocity is shown in Fig. 5. As the freestream velocity increases, the mass burning rate increases. However, near the critical value at which the transition from envelope flame occurs, there is a sudden reduction in the mass burning rate, due to reduction in the flame surface area that surrounds the particle. After transition, the mass burning rate again increases with the freestream velocity. In the envelope flame regime, the mass burning rate for the case with normal gravity is always higher than that with zero gravity. However, the difference decreases as the freestream velocity is increased. At $u_\infty \approx 1$ m/s, where transition occurs for the normal gravity case, the mass burning rate is higher for the case with zero gravity. After transition (u_∞ greater than approximately 1.1 m/s), the mass burning rates for both cases are almost the same. The ratio of the mass burning rate for normal gravity (m_{1g}) to the mass burning rate for zero gravity (m_{0g}) is plotted as a function of the Froude number ($u_\infty/(gd)^{1/2}$) in Fig. 6. The ratio decreases in the envelope flame regime and becomes almost unity after transition. This is consistent with the literature [12].

Case 2: Opposing Flow

In this case, an 8 mm spherical methanol particle undergoing combustion in a mixed convective environment with buoyancy flow being opposed by the downward forced convective flow of air (see Fig. 1b) has been considered. The freestream velocities have been varied from 0.2 to 2 m/s. The corresponding freestream Reynolds numbers based on particle diameter are in the range of 100 to 1000. Figure 7 shows the flame shapes for the cases with zero and normal gravity at various freestream velocities.

At low freestream velocity (u_∞=0.2 m/s), for the case with normal gravity, the buoyancy-induced flow is strong enough to dominate the forced convective flow. As a result, the flame extends approximately 11 diameters above the particle (see Fig. 7a). The case with zero gravity, however, has a downward extending flame. As the freestream velocity is increased to approximately 0.8 m/s, the flame for the normal gravity case becomes cylindrically flattened in shape (see Fig. 7b). At a higher freestream velocity ($u_\infty \approx 1.1$ m/s), flame transition occurs for the case with zero gravity. Contrary to the aiding flow case, the normal gravity case still has an envelope flame (see Fig. 7c). At a freestream velocity of approximately 1.2 m/s, flame transition occurs for the case with normal gravity. Figure 7d shows the wake flame shapes for both cases at a freestream velocity of 1.5 m/s. As the freestream velocity is increased beyond approximately 1.8 m/s, the present numerical model predicts complete flame extinction for the case with normal gravity. This may be due to the instability that

arises because of the opposed interaction between forced and natural convective flow fields. The case with zero gravity has a wake flame at a freestream velocity of 2 m/s. The variations of flame stand-off distances (h_1/d, h_2/d and h_3/d, as shown in Fig. 1b) with the freestream velocity are shown in Fig. 8 (a-c). These variations have an entirely different pattern when compared to the aiding flow configuration.

The flow field is also significantly affected by gravity. Figure 9 shows the streamlines at various freestream velocities for both cases. The cases with normal gravity have larger recirculation zones, especially when the flame extends upward (at low freestream velocities), as shown in Fig. 9a.

Figure 10 shows the variation of the mass burning rate (kg/s) with freestream velocity for the cases with zero and normal gravity. Obviously, the variation pattern for the zero gravity case is identical to the aiding flow case. The case with normal gravity exhibits an entirely different variation pattern. The increasing freestream velocity gradually overcomes the opposing buoyancy-induced flow. As a result, a minimum in the mass burning rate is reached, followed by an increase with further increase in the freestream velocity. Around a freestream velocity of 1.2 m/s, transition from an envelope flame to a wake flame occurs. It should be noted that unlike the aiding flow case, the mass burning rate for the normal gravity case is lower than that of the zero gravity case for freestream velocities greater than approximately 0.45 m/s.

The ratio of the mass burning rate for normal gravity (m_{1g}) to the mass burning rate for zero gravity (m_{0g}) is plotted as a function of the Froude number ($u_\infty/(gd)^{1/2}$) in Fig. 11. The ratio steeply decreases with increasing u_∞, reaches a minimum of approximately 0.75 and increases gently to unity with further increase in u_∞, except for the anomaly around $u_\infty = 1.2$ m/s due to flame transition.

Case 3: Perpendicular Flow

In this case, a semi-infinite methanol fuel film with length (L) 7.5 cm undergoing combustion within a mixed convective environment of air and with the buoyancy flow field perpendicular to the forced convective flow (see Fig.1c) has been considered. The leading edge of the fuel film starts at z/L=0.2. The freestream velocity has been varied from 0.18 to 1.4 m/s. The corresponding freestream Reynolds numbers based on the length of the fuel film are in the range of 880 to 6720.

The flame shapes are shown for different freestream velocities in Fig. 12. At a freestream velocity of 0.25 m/s (see Figs. 12a & b), the flame extent in the y direction for the normal gravity case is less than that for the zero gravity case. As a result, the temperature gradient between the flame and the fuel surface is larger for the normal gravity case, leading to a higher mass burning rate than the zero gravity case (see Fig. 13a). As the freestream velocity is increased, the gravitational strength, represented by the inverse of the Froude number ($(gL)^{1/2}/u_\infty$), decreases. This leads gradually to smaller differences in the flame shapes between zero and normal gravity cases. At a freestream velocity of 1 m/s (see Figs. 12c & d), the flame shapes are almost similar between the cases. At a freestream velocity of around 1.2 m/s (see Figs. 12e & f), the flames move away from the leading edge for both cases, because of the limitations of the chemical reaction rate to cope with the mixing rate of reactants [15]. The flame anchors at a location $z_f/L \approx 0.32$. Due to this transition in the anchoring point, the mass burning rate per unit area decreases for both cases (see Fig. 14a). At even higher freestream velocities, the flame moves further away from the leading edge (see Figs. 12g & h). The mass burning rate remains

approximately constant at the range of the higher freestream velocities considered (see Fig. 14a). At a freestream velocity value of approximately 1.5 m/s, the flame completely moves away from the computational domain. The variation of the flame anchoring position with freestream velocity is shown in Fig. 13. The variation pattern qualitatively agrees with the experimental results of Li et al. [16].

The variation of the mass burning rate per unit area (kg/m^2s) with freestream velocity is shown in Fig. 14a. The mass burning rate increases with freestream velocity for both zero and normal gravity cases, reaches a maximum around $u_\infty \approx 1.1$ m/s, slightly decreases when the flame anchoring position moves away from the leading edge around $u_\infty \approx 1.2$ m/s and remains approximately constant after that. As in the aiding flow configuration, the mass burning rate for the zero gravity case is lower than that for the normal gravity case and the difference decreases with increasing freestream velocity (see Fig. 14b)

4 Conclusions

The present study discussed the effect of gravity-induced buoyancy flow on the characteristics of diffusion flames burning within a forced convective environment. The gravitational field considerably changes the flow field, flame shapes and fuel burning rates, especially for the opposing flow case.

For the aiding flow case, the effect of gravity caused flame transition at a lower freestream velocity when compared to the zero gravity case. Also, the mass burning rates were higher for the normal gravity case before the transition to wake flame and were almost the same after transition.

For the opposing flow case, the mass burning rate for the normal gravity case was greater than the zero gravity case, only when the flame extended in the upward direction (low freestream velocity); the mass burning rates were lower for the normal gravity case at other freestream velocities. Since the forced and natural convection oppose each other, the mass burning rate attains a minimum value for the normal gravity case.

For the perpendicular flow case, the mass burning rate increases with freestream velocity while the flame is anchored right at the leading edge, both for the zero and for the normal gravity cases. As in the aiding flow configuration, the normal gravity case had a higher mass burning rate because the flame is established closer to the fuel surface. The difference in the mass burning rate between the zero and the normal gravity cases decreases with increasing freestream velocity. At higher freestream velocities (approximately greater than 1.0 m/s) the flame shapes for the zero and the normal gravity cases are almost the same. At a freestream velocity around 1.2 m/s, the flame moves away from the leading edge causing a decrease in the mass burning rate. At even higher freestream velocities, the flame moves further away from the leading edge. The mass burning rate values remain approximately constant at the range of the higher freestream velocities considered.

References

[1] Emmons H, "The Film Combustion of Liquid Fuel," *Z. Agnew. Math. Mecg.* Vol. 36, 1956, pp. 60-71.

[2] Isoda, H. and Kumagai, S., "Combustion of fuel droplets in a falling chamber," *Sixth Symposium (International) on Combustion, Combustion Institute*, 1955, pp. 726-731.

[3] Chervinsky, A., "Transient burning of spherical symmetric fuel droplets," *Israel Journal of Technology*, Vol. 7, 1969, pp. 35-42.

[4] Kumagai, S., Sakai, T. and Okajima, S., "Combustion of free fuel droplets in a freely falling chamber," *Thirteenth Symposium (International) on Combustion, Combustion Institute*, 1971, pp.779-785.

[5] Dwyer, H. A. and Sanders, B. R., "A detailed study of burning fuel droplets," *Twenty-First Symposium (International) on Combustion, Combustion Institute*, 1986, pp. 633-639.

[6] Brzustowski, T. A. and Natarajan, R., "Combustion of aniline droplets at high pressures," *The Canadian Journal of Chemical Engineering,* 44, 1966, pp.194-201.

[7] Gollahalli, S. R. and T. A. Brzustowski, "Experimental studies on the flame structure in the wake of a burning droplet," *Fourteenth Symposium (International) on Combustion, Combustion Institute,* 1973, pp.1333-1344.

[8] Balakrishnan, P., Sundararajan, T. and Natarajan, R., "Combustion of a fuel droplet in a mixed convective environment," *Combustion Science and Technology*, Vol. 163, 2001, pp. 77-106.

[9] Pope. D. N. and Gogos, G., "Numerical Simulation of Fuel Droplet Extinction Due to Forced Convection," *Combustion and Flame*, Vol. 142, 2005, pp. 89-106.

[10] Raghavan, V., Babu, V., Sundararajan, T. and Natarajan, R., "Flame Shapes and Burning Rates of Spherical Fuel Particles in a Mixed Convective Environment," *International Journal of Heat and Mass Transfer*, Vol. 48, 2005, pp. 5354–5370.

[11] Sato, J., Tsue, M., Niwa, M. and Kuno, M., "Effect of natural convection on high pressure droplet combustion," *Combustion and Flame*, Vol. 82, 1990, pp.142-150.

[12] Ling, W., H. and Chiun, H., "Single droplet combustion in a gravitational environment," *Heat and Mass Transfer*, Vol. 29(7), 1994, pp.415-423.

[13] Hirano, T., Iwai, K. and Kanno, Y., "Measurement of the velocity distribution in the boundary layer over a flat plate with a diffusion flame," *Astronautica Acta*, Vol. 17, 1972, pp. 811–818.

[14] Brahmi, L., Vietoris, T., Torero, J., L. and Joulain, P., "Estimation of boundary layer diffusion flame temperatures by means of an infrared camera under microgravity conditions," *Measurement Science and Technology*, Vol. 10, 1999, pp. 859-865.

[15] Ramachandra, A. and Raghunandan, B. N., "Investigations on the Stability and Extinction of a Laminar Diffusion Flame over a Porous Plate," *Combustion Science and Technology*, Vol. 36, 1984, pp.109-121.

[16] Li, Y., H., Dunn, R. D. and Chao, Y., C., "Burning Liquid Fuel Films from Flat Plates," *Proceedings of 20th International Colloquium on the Dynamics of Explosions and Reactive Systems*, Montreal, Canada, 2005.

[17] Agoston, G. A., Henry Wise and W. A. Rosser, "Dynamic factors affecting the combustion of liquid spheres," *Sixth Symposium (International) on Combustion, Combustion Institute*, 1957, pp. 708-717.

[18] Spalding, D. B., "Experiments on the Burning and Extinction of Liquid Fuel Spheres," *Fuel*, 32, 1957, pp. 169-185.

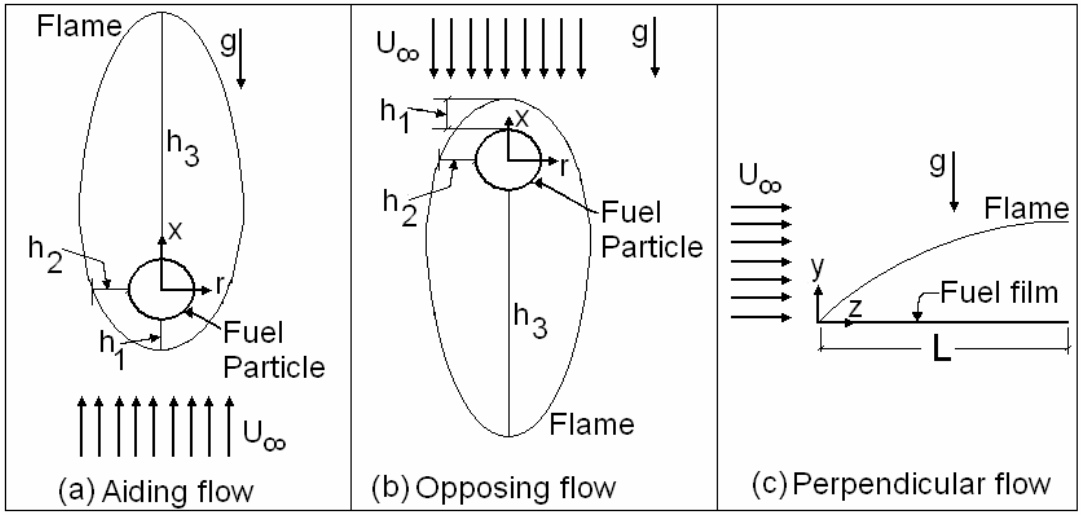

Fig.1 Configurations considered in the present study

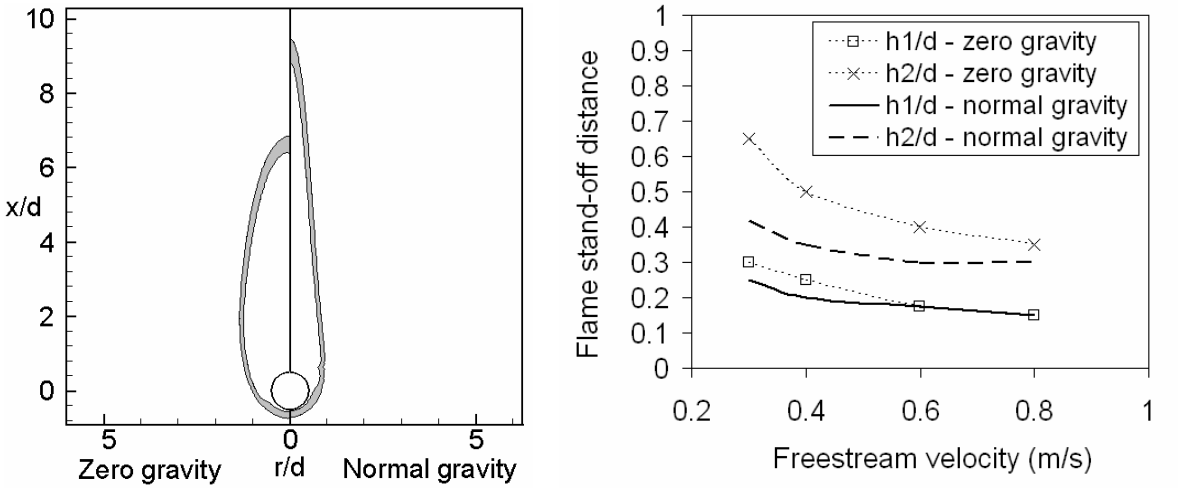

(a) u_∞=0.4 m/s, Re_∞=200 (b)

Fig. 2 Flame shapes and flame stand-off distances for envelope flame regime for aiding flow

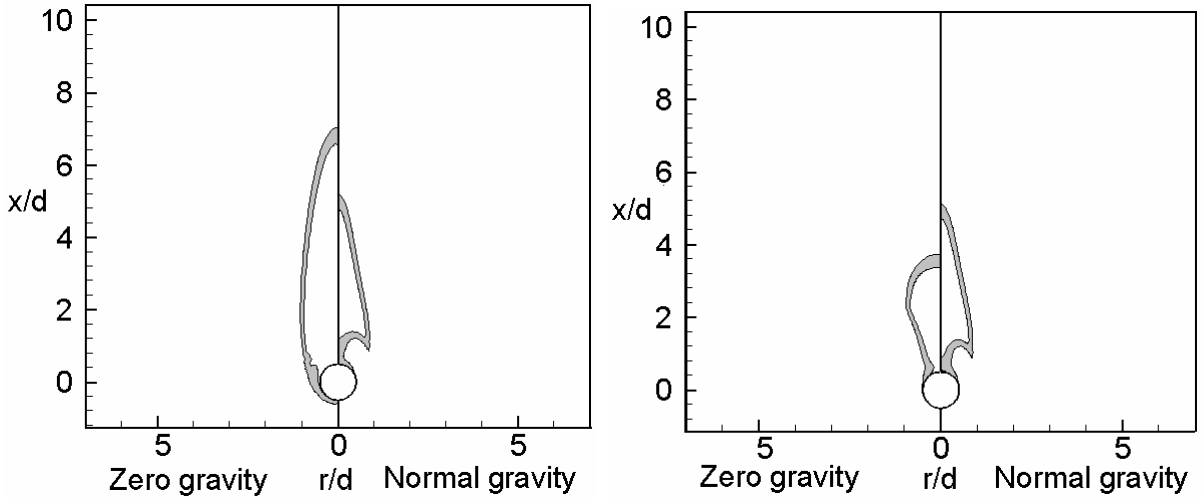

(a) u_∞=1.0 m/s, Re_∞=500 (b) u_∞=1.1 m/s, Re_∞=550

Fig. 3 (a & b) Flame shapes and flame height at various freestream velocities for aiding flow

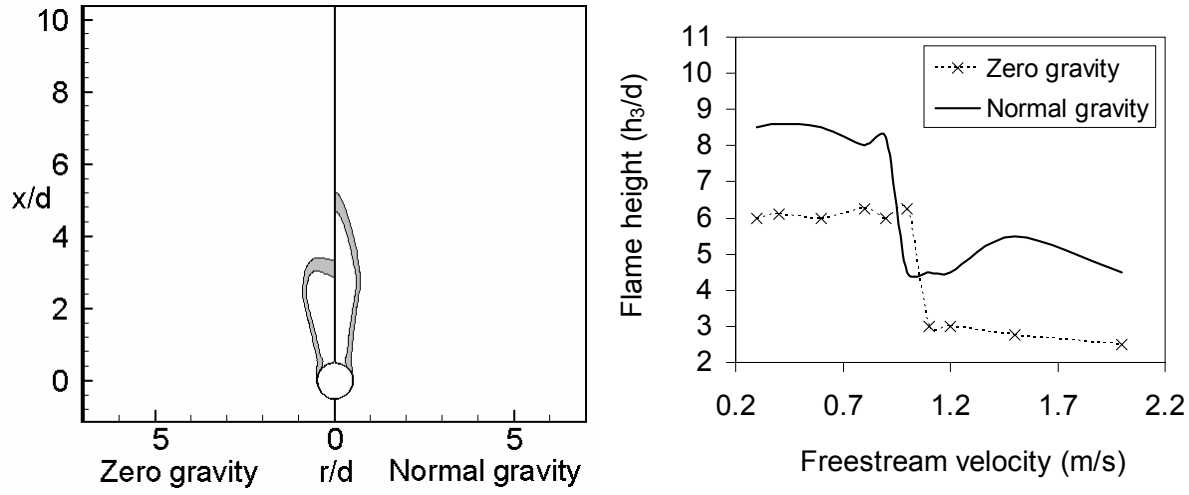

(c) u_∞=2.0 m/s, Re_∞=1000 (d)

Fig. 3 (c & d) Flame shapes and flame height at various freestream velocities for aiding flow

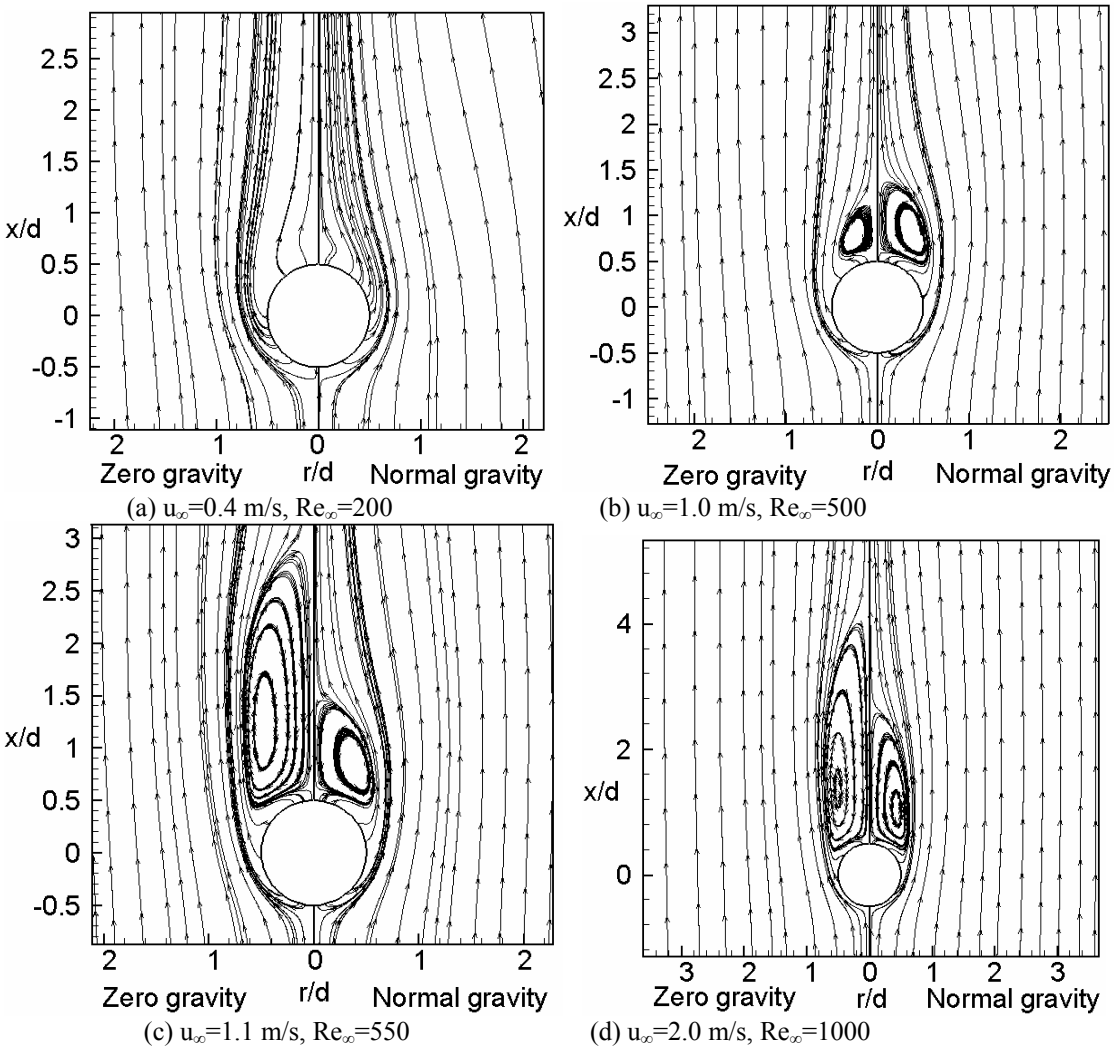

(a) u_∞=0.4 m/s, Re_∞=200 (b) u_∞=1.0 m/s, Re_∞=500

(c) u_∞=1.1 m/s, Re_∞=550 (d) u_∞=2.0 m/s, Re_∞=1000

Fig. 4 Streamlines at various freestream velocities for aiding flow

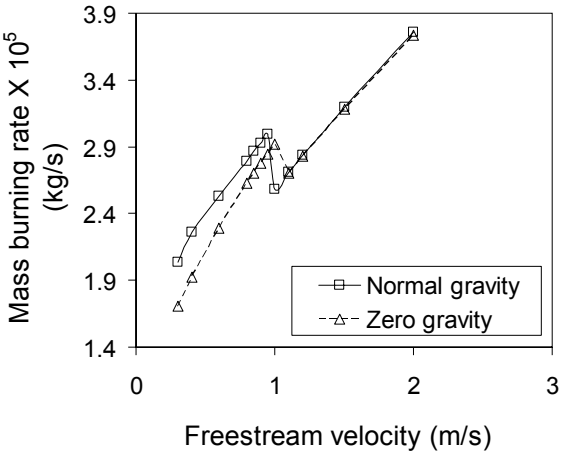

Fig. 5 Variation of mass burning rate with freestream velocity for aiding flow

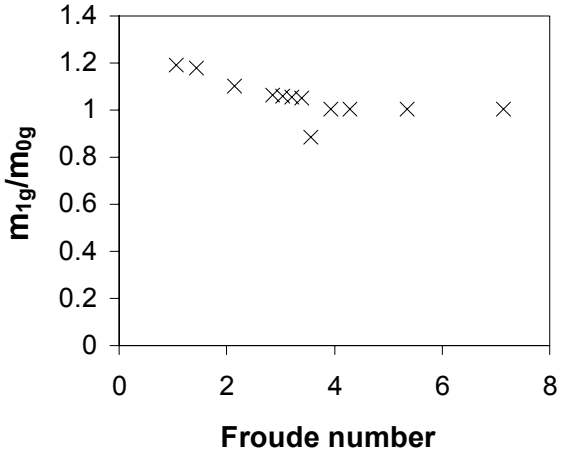

Fig. 6 Variation of the ratio of the mass burning rates with the Froude number ($u_\infty/(gd)^{1/2}$) for aiding flow

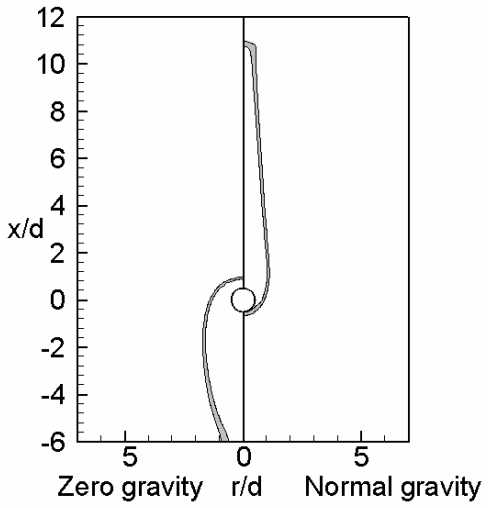

(a) u_∞=0.2 m/s, Re_∞=100

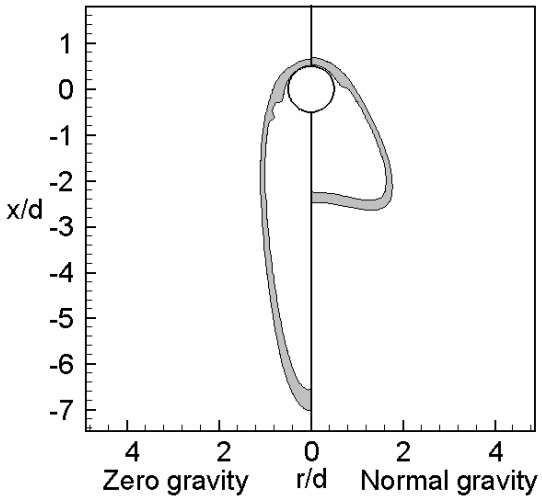

(b) u_∞=0.8 m/s, Re_∞=400

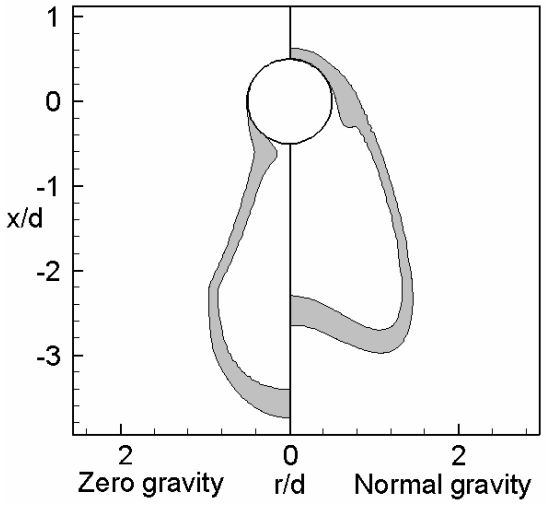

(c) u_∞=1.1 m/s, Re_∞=550

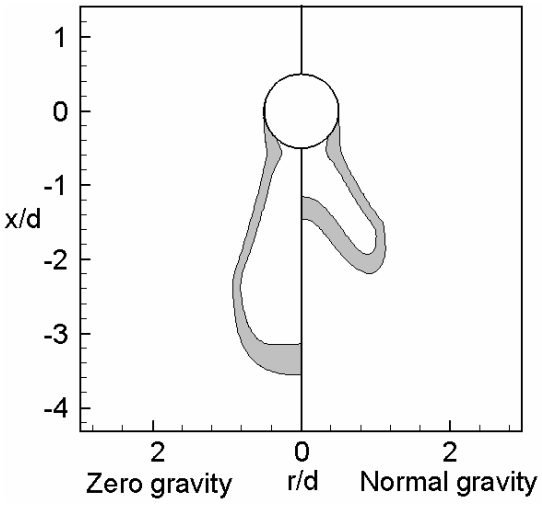

(d) u_∞=1.5 m/s, Re_∞=750

Fig. 7 Flame shapes at various freestream velocities for opposing flow

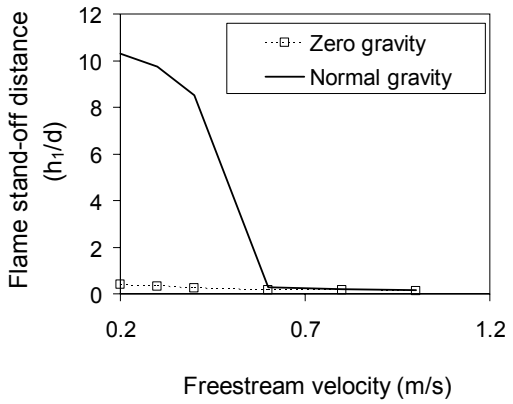

(a) h_1/d vs. u_∞

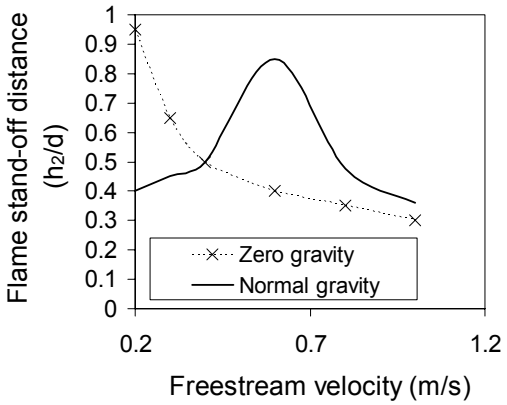

(b) h_2/d vs. u_∞

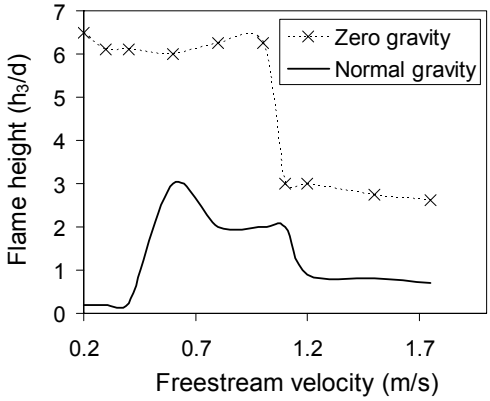

(c) h_3/d vs. u_∞

Fig. 8 Flame stand-off distances for opposing flow

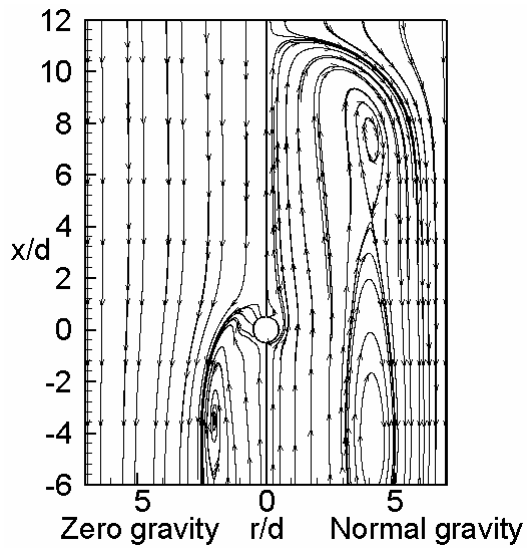

(a) u_∞=0.2 m/s, Re_∞=100

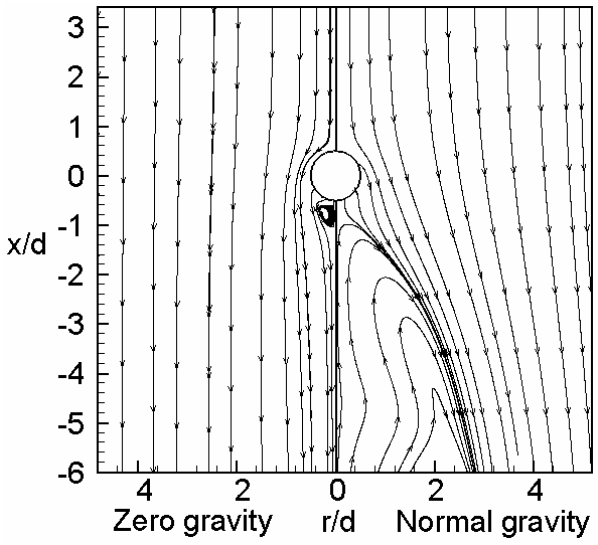

(b) u_∞=0.8 m/s, Re_∞=400

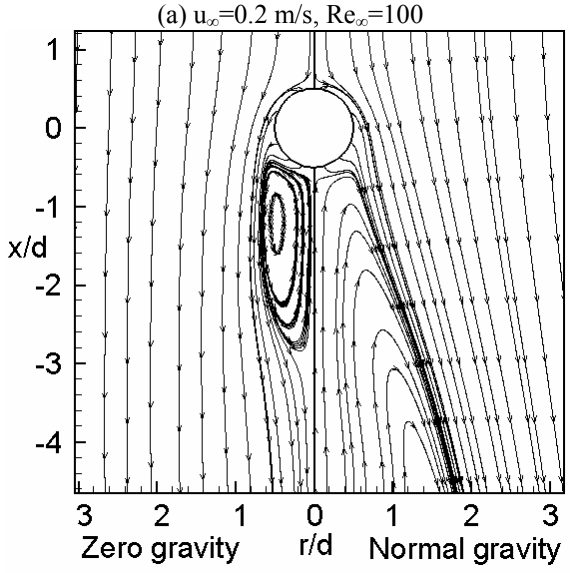

(c) u_∞=1.1 m/s, Re_∞=550

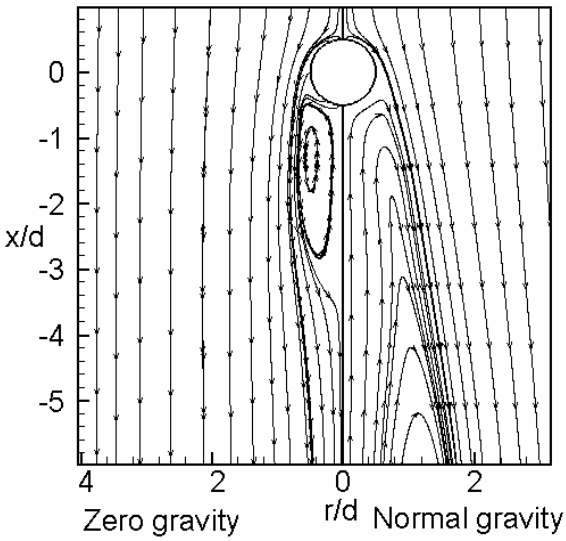

(d) u_∞=1.5 m/s, Re_∞=750

Fig. 9 Streamlines at various freestream velocities for opposing flow

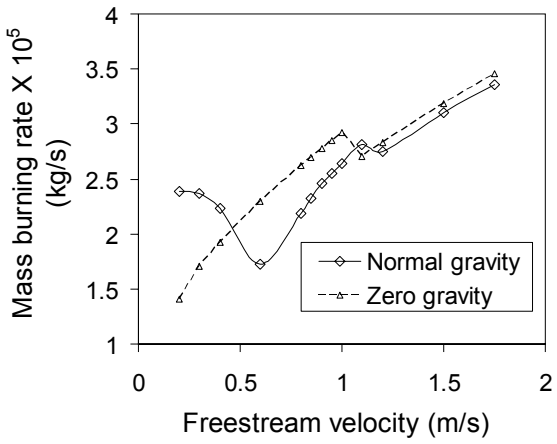

Fig 10 Variation of the mass burning rate with freestream velocity for opposing flow

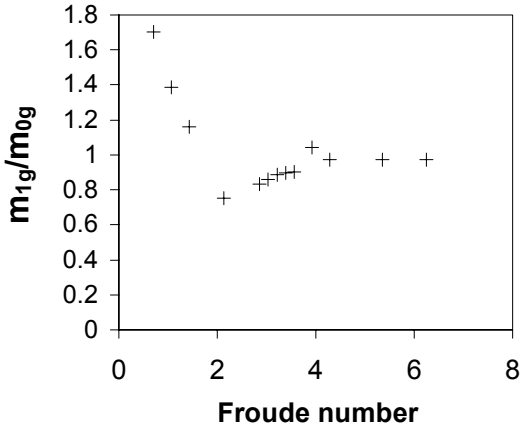

Fig. 11 Variation of the ratio of the mass burning rate with the Froude number ($u_\infty/(gd)^{1/2}$) for opposing flow

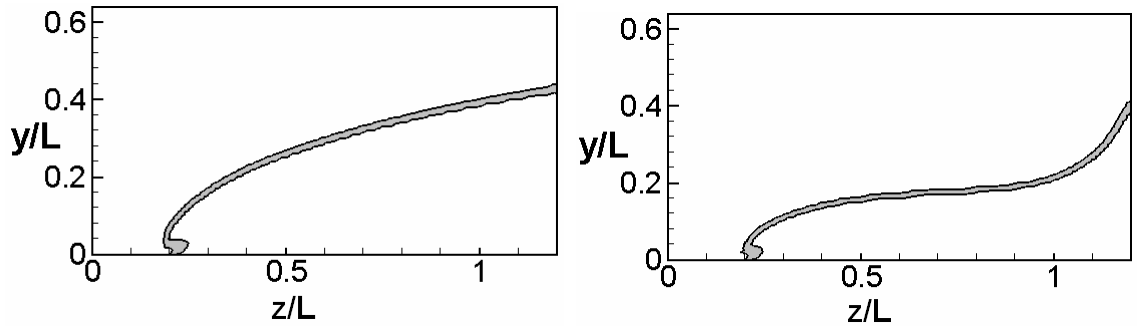

(a) u_∞=0.25 m/s, Re_∞=1200, zero gravity (b) u_∞=0.25 m/s, Re_∞=1200, normal gravity

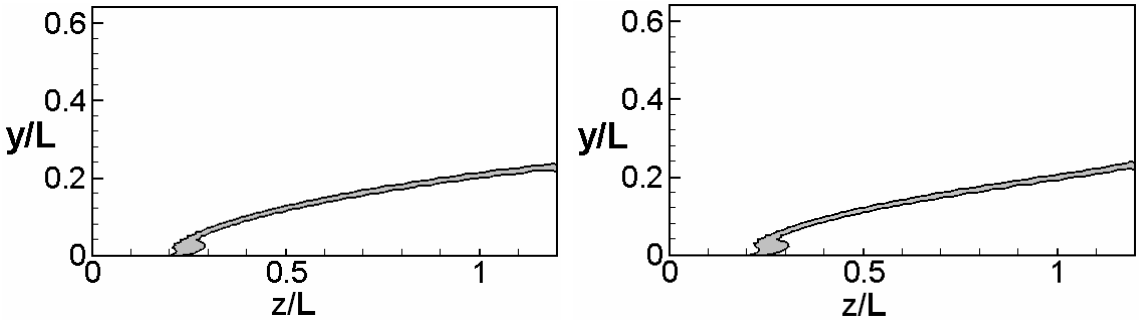

(c) u_∞=1 m/s, Re_∞=4800, zero gravity (d) u_∞=1 m/s, Re_∞=4800, normal gravity

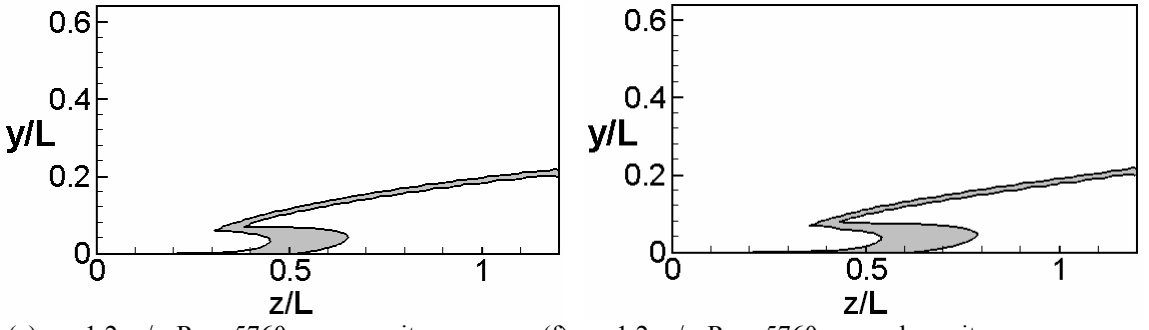

(e) u_∞=1.2 m/s, Re_∞=5760, zero gravity (f) u_∞=1.2 m/s, Re_∞=5760, normal gravity

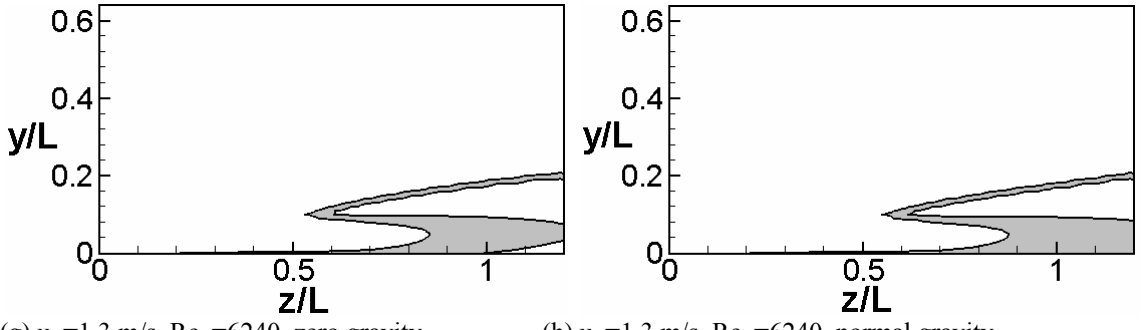

(g) u_∞=1.3 m/s, Re_∞=6240, zero gravity (h) u_∞=1.3 m/s, Re_∞=6240, normal gravity

Fig. 12 Flame shapes at various freestream velocities for the perpendicular flow case

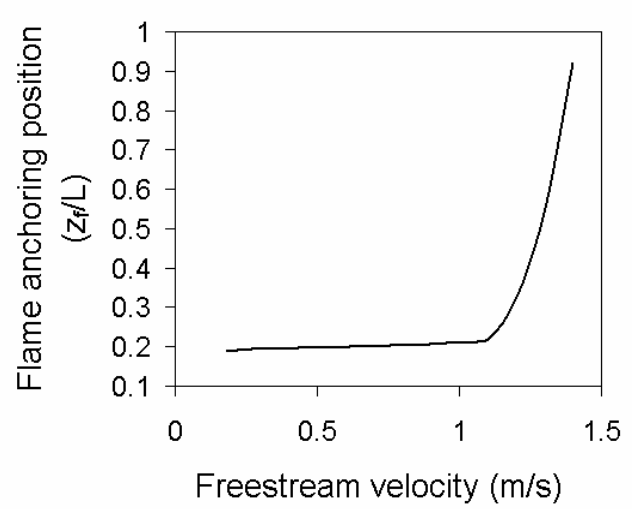

Fig. 13 Variation of flame anchoring position with freestream velocity for perpendicular flow

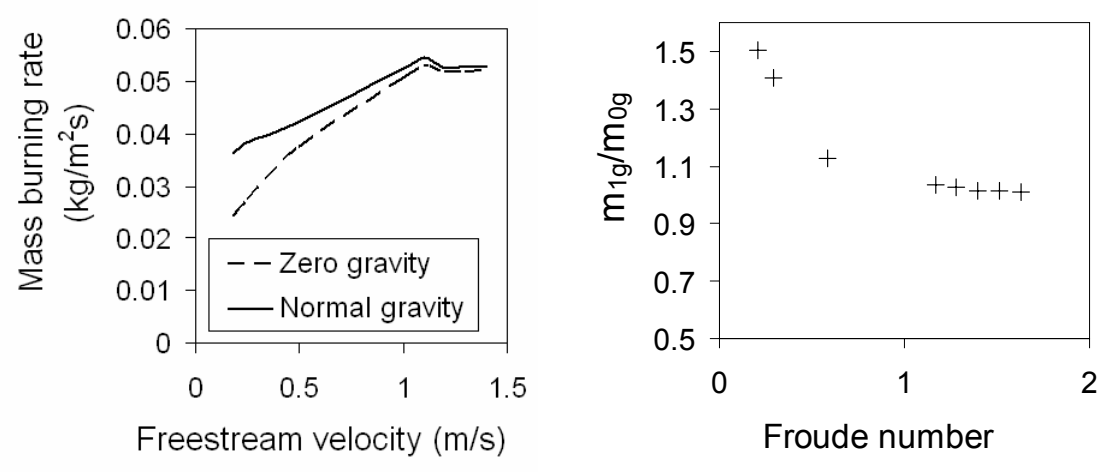

(a) (b)

Fig 14 (a) Mass burning rate per unit area vs. u_∞ and (b) Ratio of the mass burning rates vs. Froude number $(u_\infty/(gd)^{1/2})$ for perpendicular flow